Synthesis of Azahexabenzocoronenium Enabled by Formal [3+3] Cycloaddition Strategy

Xinjiang Zhang,[1] Donglin Li,[2] Cheryl Cai Hui Tan,[1] Fiona Hanindita,[1] Yosuke Hamamoto,[1] Adam S. Foster,[4,5,*] Shigeki Kawai[2,3,*] & Shingo Ito[1,*]

[1] *School of Chemistry, Chemical Engineering and Biotechnology, Nanyang Technological University, 21 Nanyang Link, Singapore 637371, Singapore*

[2] *Center for Basic Research on Materials, National Institute for Materials Science, 1-2-1 Sengen, Tsukuba, Ibaraki 305-0047, Japan*

[3] *Graduate School of Pure and Applied Sciences, University of Tsukuba, Tsukuba 305-8571, Japan*

[4] *Department of Applied Physics, Aalto University, P.O. Box 11100, Aalto, Espoo 00076, Finland*

[5] *Nano Life Science Institute (WPI-NanoLSI), Kanazawa University, Kakuma-machi, Kanazawa 920-1192, Japan*

Abstract

Heteroatom-embedded hexa-*peri*-hexabenzocoronene (HBC) molecules exhibit interesting properties depending on the number and position of the introduced heteroatoms and are promising materials for applications in organic electronics and supramolecular chemistry. However, their synthesis is quite limited because of the difficulty in selectively introducing heteroatoms into the HBC core, which poses a new challenge in organic synthesis. In this study, we report a novel synthetic strategy for the in-solution synthesis of 3a^2-azahexa-*peri*-hexabenzocoroneniums, which are cationic nitrogen-embedded HBC derivatives. The synthesis was enabled by formal [3+3] cycloaddition of polycyclic aromatic azomethine ylides with cyclopropenes as a 3-atomic dipolarophile followed by mechanochemical intramolecular cyclization. Furthermore, on-surface polymerization of aza-HBC precursors was performed to synthesize aza-HBC-based corrugated graphene nanoribbons. This study provides new possibilities for the utilization of nitrogen-embedded HBC derivatives in a variety of potential applications.

Introduction

Hexa-*peri*-hexabenzocoronene (HBC; **Fig. 1**) is a discotic polycyclic aromatic molecule composed of 42 carbon atoms and 18 hydrogen atoms. Since its first synthesis in 1958,[1,2] HBC and its derivatives have emerged as the most prominent representative of polycyclic aromatic molecules because of their extended π-conjugated surface, characterized by regularly aligned benzenoid hexagons.[3,4,5] The fascinating symmetrical structure and intriguing properties of HBC have fueled extensive research on its

synthesis and applications in supramolecular chemistry,[6,7] organic electronics,[3,4,5,8,9] and biology.[10,11]

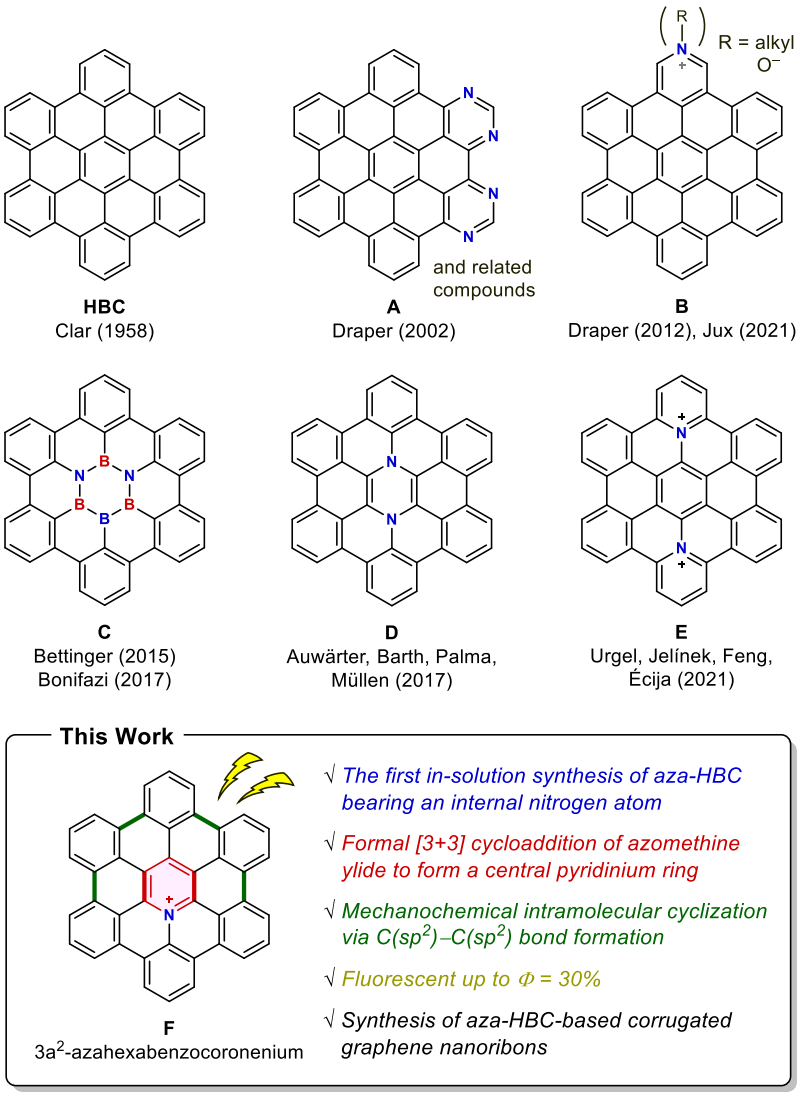

Fig. 1. Hexa-*peri*-hexabenzocoronene (HBC) and nitrogen-embedded HBC molecules in the literature (A–E) and in this work (F).

Given the profound significance of HBC molecules, the exploration of heteroatom-embedded HBC molecules presents a compelling avenue for research across a wide range of scientific disciplines.[12,13,14] The first synthesis of a nitrogen-containing HBC molecule was reported in 2002, when Draper successfully developed pyrimidine-fused HBCs (**A**) and their application as ligands in organometallic chemistry.[15,16,17] Later, Draper[18] and Jux[19] independently introduced a novel class of HBCs fused with a peripheral pyridine ring (**B**), which were subsequently converted to cationic analogs such as alkylpyridinium and pyridine oxide. While these HBC molecules feature nitrogen atoms at their periphery, the incorporation of heteroatoms into the internal framework remains an intricate and formidable challenge. The synthesis of HBC molecules with internal heteroatoms has been achieved mainly by on-surface synthesis, as exemplified by borazine-embedded HBC (**C**) in 2015,[20] pyrazine-

embedded HBC (**D**) in 2017,[21] and pyridinium-embedded HBC (**E**) in 2021,[22] although the in-solution synthesis of **C** was later reported by the group of Bonifazi.[23,24] It is important to note that on-surface synthesis, while feasible, inherently restricts the comprehensive investigation of their properties and hampers their practical application. Consequently, there is a pressing need for in-solution organic synthesis of heteroatom-embedded HBC molecules. Herein, we report the in-solution synthesis of novel cationic nitrogen-embedded hexabenzocoronene derivatives **F**, namely 3a^2-azahexa-*peri*-hexabenzocoronenium. The synthesis was achieved through a formal [3+3] cycloaddition of polycyclic aromatic azomethine ylides and cyclopropenes, which act as "3-atomic dipolarophiles", followed by mechanochemical intramolecular cyclization, facilitating the formation of C(sp^2)–C(sp^2) bonds. The structure and properties of azahexabenzocoronenium **F** were investigated by various spectroscopic methods, which have been difficult to perform with other heteroatom-embedded HBC molecules bearing internal heteroatoms.

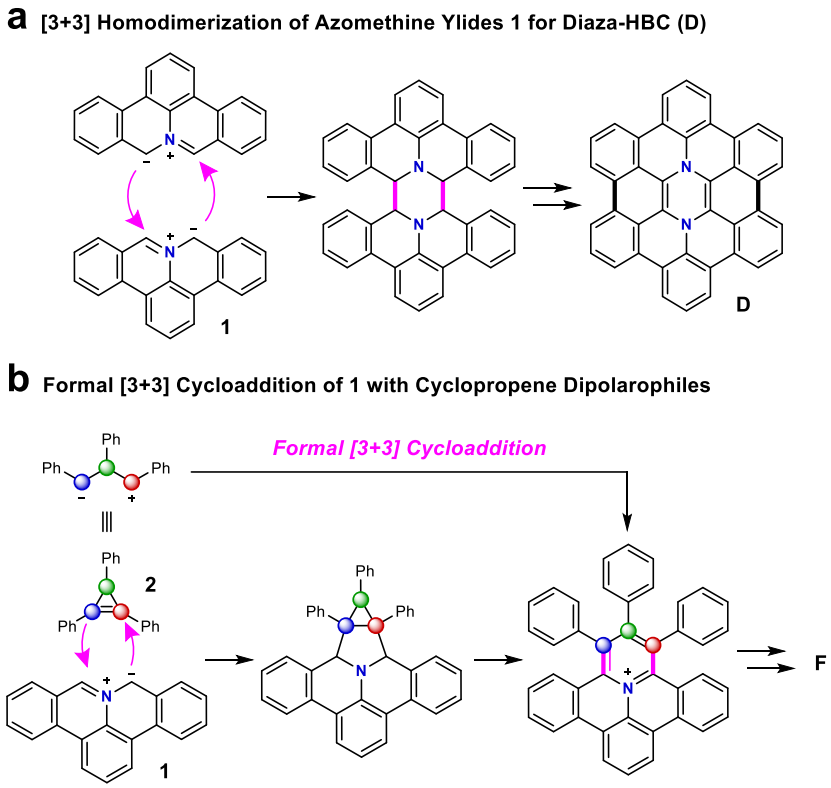

Fig. 2. 1,3-Dipolar cycloaddition of azomethine ylides to form nitrogen-embedded HBC derivatives. **a**, [3+3] Homodimerization of azomethine ylide to form pyrazine-embedded HBC **D**.[21] **b**, Formal [3+3] cycloaddition of azomethine ylides and cyclopropenes as 3-atomic dipolarophiles.

Fig. 2 illustrates our synthetic design for cationic HBC molecule **F**, which is based on the 1,3-dipolar cycloaddition of polycyclic aromatic azomethine ylides **1**.[25,26,27,28,29,30,31,32] It was previously reported that HBC molecule **D** was synthesized through [3+3] homodimerization of azomethine ylides **1** followed by oxidative cyclization on the metal surface (**Fig. 2a**).[21] In our initial approach, therefore, we planned to adopt the same 1,3-dipolar cycloaddition strategy to synthesize azahexabenzocoronenium **F**.

To construct its core structure, we need to perform [3+3] cycloaddition of azomethine ylide **1** with a 3-atomic CCC unit (**Fig. 2b**), but this type of [3+3] cycloaddition reaction has never been reported. Consequently, we decided to develop a formal [3+3] cycloaddition using cyclopropene derivative **2** as a coupling partner. Since **2** is an alkene molecule, it can undergo 1,3-dipolar cycloaddition with polycyclic aromatic azomethine ylides **1** to yield the corresponding cycloadduct. The resulting bicyclo[3.1.0]hexane system is expected to undergo skeletal rearrangement upon oxidation, forming the corresponding pyridinium ring.[33,34] Overall, this transformation can be considered a formal [3+3] cycloaddition of azomethine ylide **1** and cyclopropene **2**, with the latter serving as a 3-atomic dipolarophile, ultimately leading to the formation of azahexabenzocoronenium **F**.

Results and discussion

To validate our hypothesis, 1,3-dipolar cycloaddition of a polycyclic aromatic azomethine ylide derived from iminium salt **1a** and cyclopropene derivative **2a**[35] was performed in chloroform at 60 °C, which yielded cycloadduct **3a** in nearly quantitative yield as a mixture of diastereomers with a ratio of 70:28 (**Fig. 3a**). The high reactivity of **2a** as an alkene leading to the high yield of **3a** is attributed to its inherent molecular strain in the cyclopropene structure.[30] The diastereomers of **3a** can be separated and isolated by silica gel column chromatography and further characterized by NMR analyses, mass analyses, and single crystal X-ray diffraction analysis (**Supplementary Fig. 65**). Subsequently, **3a** was treated with 3.0 equivalents of chloranil, which serves as an oxidant, at 40 °C. This treatment induced a skeletal rearrangement, converting azabicyclo[3.1.0]hexane into the corresponding pyridinium ring. Notably, both isomers of **3a** underwent this transformation with high efficiency, providing π-extended pyridinium **4a** in high yields. This reaction was found to be versatile because it was successfully applied to a wide range of substrates (**Fig. 3b**). Cyclopropene substrates bearing electron-donating and electron-withdrawing groups afforded **4b**–**4d** in good yields. Additionally, the phthalimide functionality was compatible under the reaction conditions to produce **4e**, indicating that alkyl substituents can also be introduced instead of alkoxycarbonyl and aryl groups. The generality of the reaction conditions was further demonstrated with various 1,2,3-triarylcyclopropene substrates, leading to the formation of 1,2,3-triarylated dibenzoullazine molecules **4f**–**4o** in high yields.

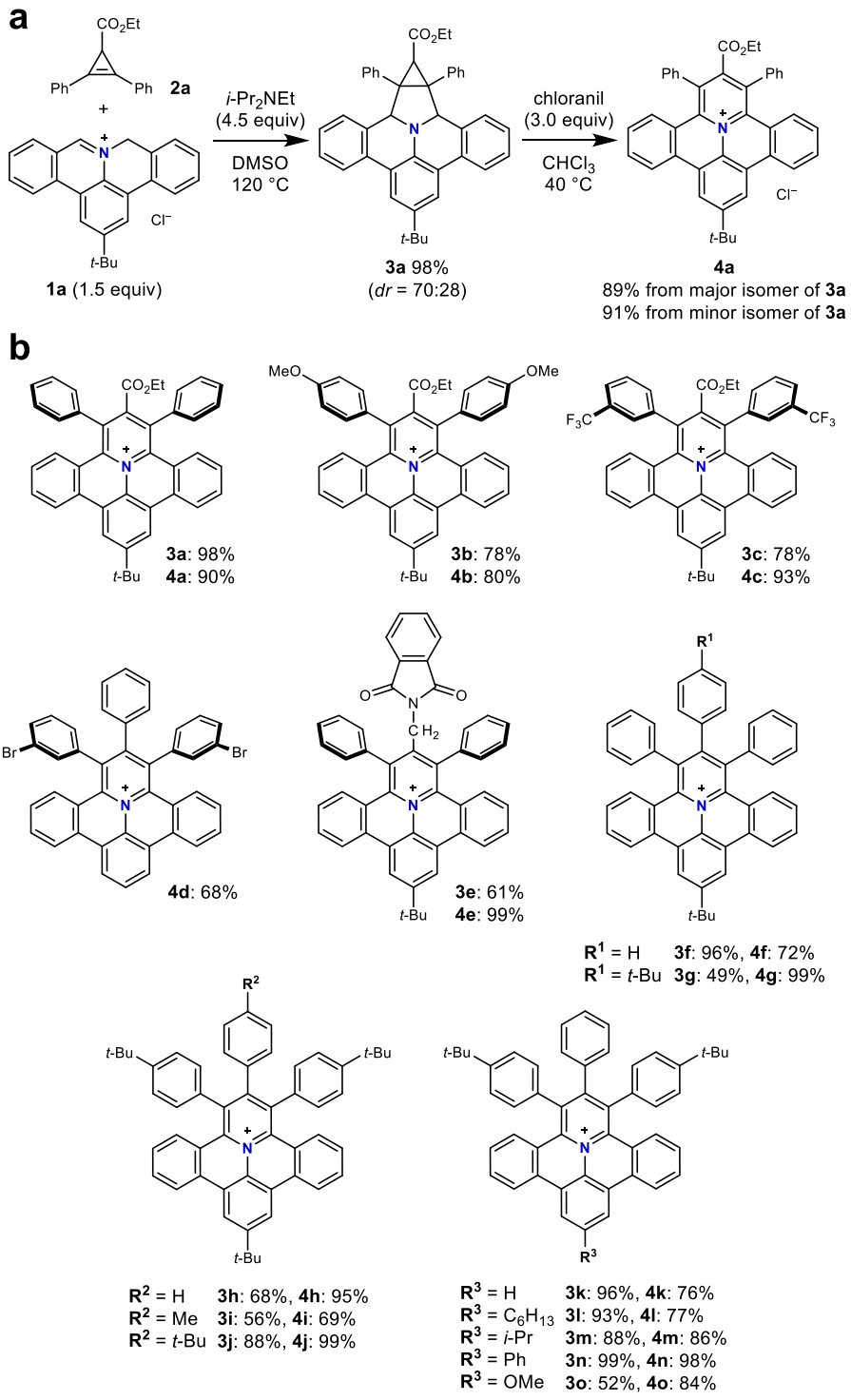

Fig. 3. Synthesis of π-extended pyridinium derivatives. a, 1,3-Dipolar cycloaddition of azomethine ylides and cyclopropenes followed by oxidative skeletal rearrangement. **b**, Substrate scope. Counterions are omitted for clarity.

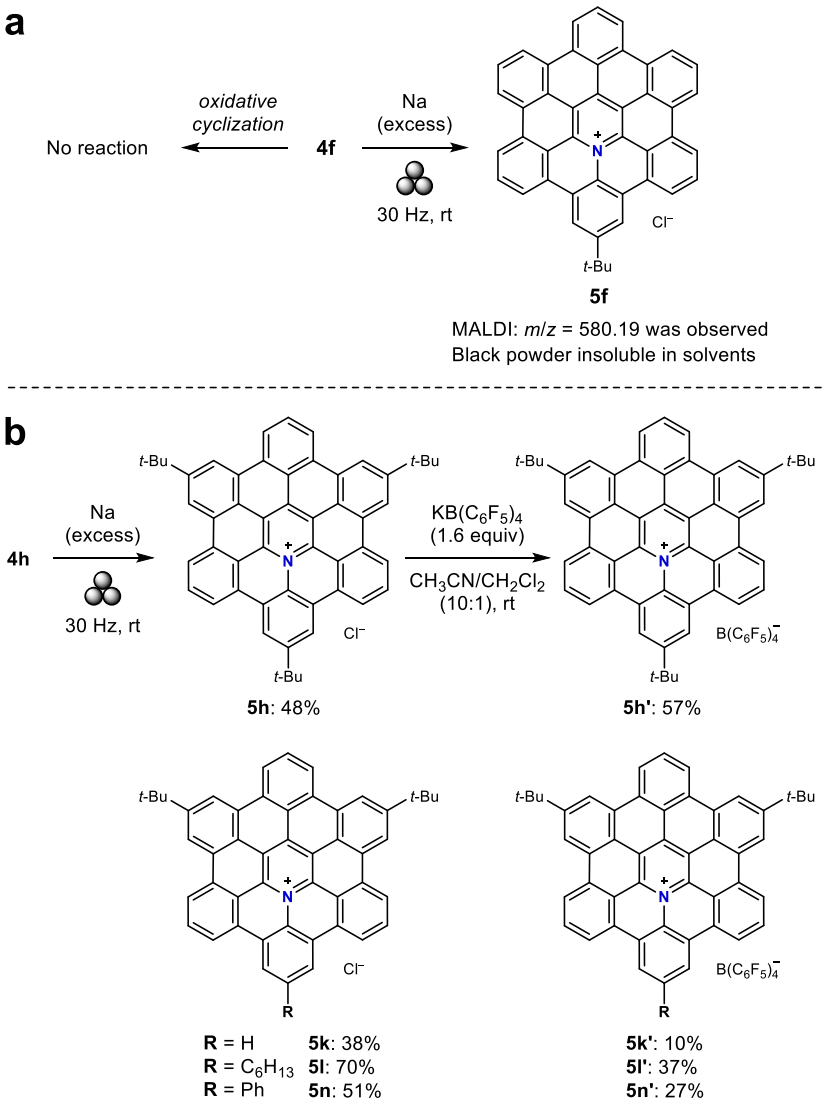

Fig. 4. Synthesis of azahexabenzocoronenium. **a**, Attempted synthesis of **5f** by mechanochemical cyclization. **b**, Synthesis of **5h** and an anion exchange reaction leading to **5h'**.

The molecular shape of π-extended pyridinium salts **4f–o** prompted us to examine a dehydrogenative cyclization approach to afford azahexabenzocoronenium **5**, *i.e.*, 3a^2-azahexabenzo[*bc*,*ef*,*hi*,*kl*,*no*,*qr*]coronenium (**Fig. 4**). In the initial trials, Scholl reactions of **4f** using various oxidative conditions were performed, since it is a well-established strategy for promoting the cyclodehydrogenation of polycyclic aromatic molecules.[36,37,38] However, none of the oxidative conditions successfully afforded **5**, presumably because the electron-deficient nature of the pyridinium precursors hampered oxidation reactions (**Fig. 4a**; left). We then shifted our focus to cyclization under reductive conditions,[39,40,41,42] which is often facilitated by mechanochemistry (**Fig. 4a**; right).[43] Accordingly, the four-fold cyclodehydrogenation of **4f** was performed in the presence of excess sodium (Na) under ball milling (30 Hz) at room temperature, resulting in the formation of a black powder as a product. The MALDI-TOF mass spectrum of the crude mixture showed only signals at *m*/*z* = 580.19, which corresponds to the target molecule, azahexabenzocoronenium **5f**. However, the black powdery

product did not dissolve in any solvents and could not be purified. In the next trial, therefore, we turned our attention to **4h**, which bears three *tert*-butyl groups, aimed at enhancing the solubility (**Fig. 4b**). As anticipated, the reaction of **4h** proceeded well to produce **5h**, which shows significantly improved solubility in organic solvents. Due to the poor crystallinity of **5h** bearing chloride as the counterion, we performed a counterion exchange reaction to obtain the corresponding borate salt, **5h'**. Likewise, we conducted mechanochemical reductive cyclization to **4k**, **4l**, and **4n**, each featuring different substituents. These efforts resulted in reasonable yields of **5k**, **5l**, and **5n**, respectively, expanding the scope of our synthesized compounds.

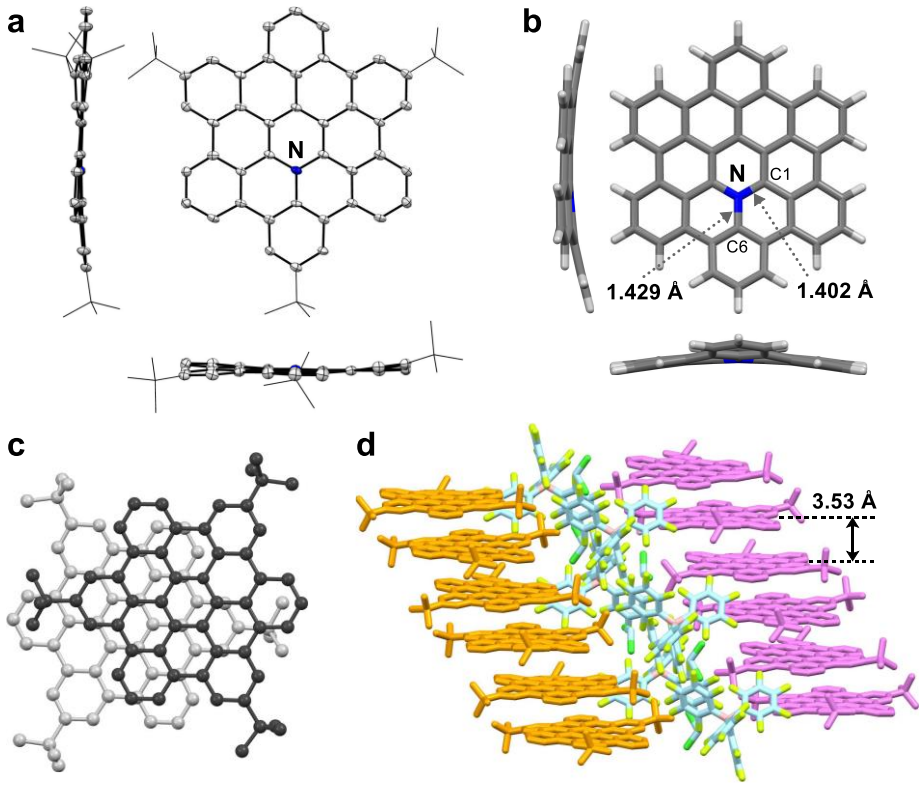

Fig. 5. Molecular structures of azahexabenzocoronenium 5h'. a, ORTEP structure of **5h'**. Hydrogen atoms are omitted, and *t*-butyl groups are shown as stick models for clarity. **b**, Structure of **5** determined by DFT calculation at the B3LYP/6-31G(d) level of theory. **c**,**d**, Packing structures of **5h'**.

Single crystals of **5h'** were obtained by recrystallization in dichloromethane and analyzed by X-ray diffraction measurement (**Fig. 5**). The **5h'** crystallizes in the *P*−1 space group with four molecules and solvent molecules in the unit cell. The cationic π-core adopts a nearly planar structure with a slight wavy distortion, likely arising from the steric interaction of the *t*-butyl groups (**Fig. 5a**). Unfortunately, however, the crystal structure contains disorder in terms of the position of the nitrogen atoms, *i.e.*, the crystal contains 1/3 of each of the three structures in **Supplementary Fig. 67** as disorder. Therefore, the central pyridinium ring is observed as a regular hexagon as a result of averaging their structures, preventing us from discussing detailed molecular structures, including bond lengths and bond angles.

Consequently, the molecular structure was determined by density functional theory (DFT) calculations at the B3LYP/6-31G(d) level of theory (**Fig. 5b**). The optimized structure in the gas phase has a shallow saddle shape, which would be attributed to the shorter carbon–nitrogen bonds (N–C1: 1.402 Å, N–C6: 1.429 Å) compared with the corresponding carbon–carbon bonds of HBC (1.424 and 1.448 Å, respectively) (**Supplementary Fig. 68**). In the crystal packing, azahexabenzocoroneniums are slip-stacked in a face-to-face manner so that each carbon atom is located near the center of a six-membered ring in the underlying molecule (**Fig. 5c**). This packing arrangement closely resembles what is observed in the crystal structure of hexa-*t*-butyl-HBC.[44] The cationic cores form oblique one-dimensional columns with an interplanar distance of 3.53 Å (**Fig. 5d**). This value is larger than that of hexa-*t*-butyl-HBC (3.44 Å)[44] and a pyridine-fused HBC-type compound (3.36 Å),[19] which is likely attributed to the electrostatic repulsion between cationic aromatic cores. There is no interaction between the columns as the space between the columns is filled with large anions, *i.e.*, $B(C_6F_5)_4^-$ and solvent molecules.

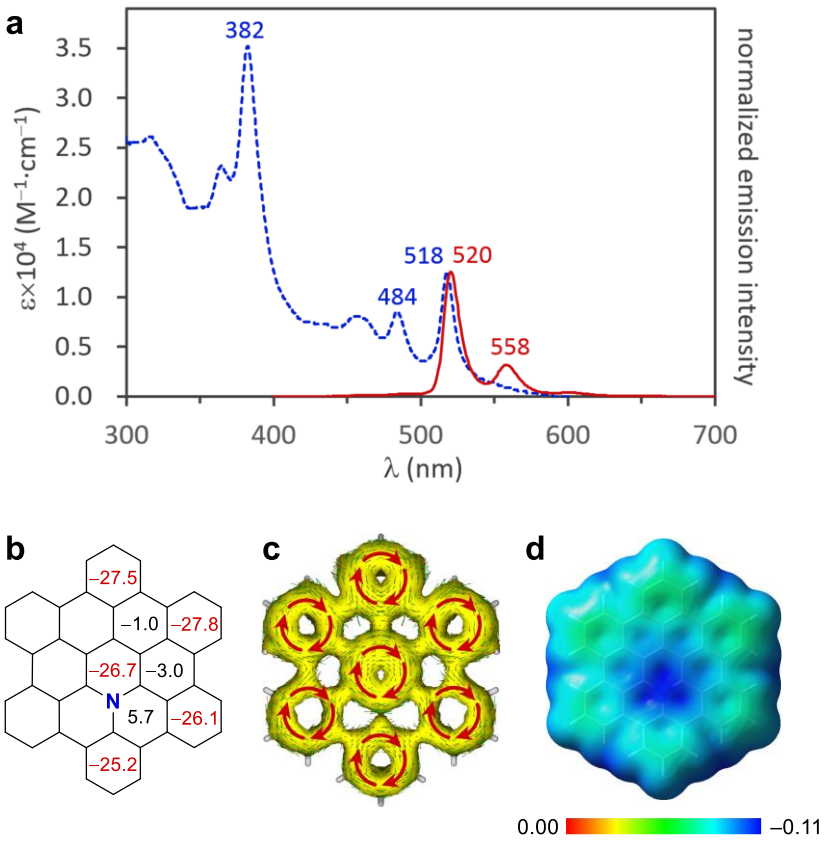

Fig. 6. Molecular properties of azahexabenzocoronenium 5. **a**, UV/visible absorption (blue dotted line) and normalized emission (red solid line; excitation wavelength: 350 nm) spectra of azahexabenzocoronenium **5h** (5.6×10^{-6} M in CH_2Cl_2). **b**, $NICS(1)_{zz}$ values of **5** (average of values on the back and front of the curved surface). **c**, ACID plot of **5**, **d**, ESP map of **5**.

The optical properties of compound **5h** were investigated (**Fig. 6a**). The absorption spectrum shows a broad absorption profile with absorption maxima at 518, 484, and 382 nm. According to time-

dependent (TD) DFT calculations, the former two absorptions correspond to the HOMO/LUMO and HOMO−1/LUMO transitions, respectively (**Supplementary Fig. 74 and Table 3**). Notably, in the case of hexabenzocoronene **1**, the observed absorption wavelength is significantly shorter (<400 nm).[45,46] This phenomenon can be attributed to the highly symmetrical structure of hexabenzocoronene, which results in the symmetrically forbidden nature of some low-energy transitions (referred to as α- and β-bands[47]), preventing them from contributing to longer wavelength absorption (**Supplementary Fig. 73 and Table 2**). Therefore, the introduction of a nitrogen atom into the HBC core disrupts its molecular symmetry, allowing these low-energy absorptions to occur.[47] Additionally, the fluorescence of **5h** was observed in the range from 500 to 650 nm, including vibrationally resolved maxima. The fluorescence pattern mirrors the longest absorption bands. Remarkably, the Stokes shift is only 2 nm, suggesting the highly rigid structure of azahexabenzocoronenium **5h**. The fluorescence quantum yield was determined to be 30%, which is higher than that of hexabenzocoronene derivatives (typically <10%).[46] This improvement in the emission quantum yield underscores the advantages of introducing nitrogen atoms into highly symmetric polycyclic aromatic molecules such as corannulene[48] and HBC,[15,17] enhancing their fluorescence properties.

The aromaticity and electronic properties of **5** were investigated by DFT calculations. Nucleus independent chemical shift (NICS) analysis revealed a value of −26.7 at the central pyridinium ring, with values ranging from −25.2 to −27.5 at the peripheral benzene rings, which indicates that they are aromatic (**Fig. 6b**). Indeed, the ACID plot shows the presence of 6π clockwise ring currents along the central pyridinium and peripheral six benzene rings (**Fig. 6c**). These findings provide compelling evidence that the aromatic nature of **5** closely resembles that of the parent HBC (**Supplementary Figs. 71 and 72**). Additionally, electrostatic map analysis indicateed that the cationic charge is localized around the internal nitrogen atom (**Fig. 6d**).

To expand the application of azahexabenzocoronenium **5**, we decided to perform its oligomerization on metal surfaces to fabricate corrugated nitrogen-containing graphene nanoribbons (GNRs; **Fig. 7a**). Several examples of HBC-based corrugated GNRs bearing nitrogen atoms in their periphery have been reported in the literature,[49,50,51,52,53,54,55] but there are fewer examples of HBC-based corrugated GNRs bearing internal nitrogen atoms.[56] Initially, precursor **4d** was sublimed *in situ* onto a clean Au(111) surface under ultrahigh vacuum conditions. The large-scale scanning tunneling microscopy (STM) image (**Fig. 7b**) shows that the cationic part of **4d** assembles into distinct small clusters, while no chlorine atoms were detected on the metal surface (**Supplementary Fig. 77**).[22] A high-resolution STM image of one of these clusters is shown in the inset of **Fig. 7b**. Subsequently, the sample underwent annealing at 150 °C, inducing an intermolecular Ullmann-type cross-coupling reaction to form the polymer intermediate (**Fig. 7c**). The high-resolution image of the polymer (inset of **Fig. 7c**) reveals a periodicity of 0.88 nm, indicating the formation of covalent bonds between the precursor molecules. The bright spots observed in the middle of the polymer chain arise from the steric effect of the out-of-plane phenyl rings. Further elevating the annealing temperature to 400 °C resulted in complete planarization of

the linear structures (**Fig. 7d**). High-resolution STM images (**Fig. 7e–g**) of these products with varying lengths demonstrate the successful synthesis of the desired oligomers depicted in **Fig. 7a**, although some oligomers with defects were also observed (**Supplementary Fig. 75**). Bond-resolved STM (BR-STM) imaging with a CO-functionalized tip (**Fig. 7h–j**) clearly confirmed the formation of the desired GNRs, providing direct and compelling evidence that the synthetic concept illustrated in **Fig. 7a** was successfully realized. It is noteworthy that the selective introduction of nitrogen atoms is ensured by a darker contrast around the nitrogen atoms, which was reported in previous studies.[22,57,58] In addition, the electronic properties of the corrugated GNRs were measured by scanning tunneling spectroscopy with a metal tip, which revealed that their band gap gradually decreased with increasing number of aza-HBC units (**Supplementary Fig. 76**). To further clarify the electronic structure and charge state of GNRs, we performed a series of theoretical calculations of pentameric GNRs with increasing numbers of positive charges using the vacuum level to align the Fermi energy between them and the ideal Au (111) surface. **Supplementary Fig. 79A**, **79B**, and **79C** show the density of states of the pentameric GNRs in the gas phase with charges of 0, +1, and +2 per 2N site unit cell, respectively. As shown in **Supplementary Fig. 80A**, the dI/dV spectrum of the pentameric GNRs on the gold surface was also calculated and found to be in the best agreement for the gas-phase system with +1 charges. This is further confirmed by calculating the charge transfer between the GNR and the gold surface (**Supplementary Fig. 80B**), where a decrease in positive charge at the nitrogen sites and an associated accumulation of positive charge at the gold site directly below it are observed. The simulated contrast in **Supplementary Fig. 80C** is in reasonable agreement with that shown in **Supplementary Fig. 76**. These results led to the conclusion that the local positive charge on each azahexabenzocoronenium unit of the GNRs is +0.5. It was reported that a dicationic diaza-HBC molecule adopts a dicationic state on the Au(111) surface,[22] and that neutral nitrogen-embedded PAH molecules adsorbed on the Au(111) surface are positively charged due to the charge transfer from the neutral molecules to the underlying metal substrate.[56,57] Given these reports, it is reasonable to conclude that the present GNRs have +0.5 charge per aza-HBC unit.

Conclusions

In summary, we have developed a new synthetic approach for accessing heteroatom-embedded hexa-*peri*-hexabenzocoronene derivatives. The key to the successful synthesis of 3a^2-azahexa-*peri*-hexabenzocoronenium lies in the formal [3+3] cycloaddition of polycyclic azomethine ylides with cyclopropene derivatives, followed by mechanochemical intramolecular cyclization. A comprehensive investigation of the optical and electronic properties of the resulting molecules was performed through spectroscopic analyses as well as theoretical calculations. Furthermore, we extended our methodology to synthesize corrugated 3a^2-azahexa-*peri*-hexabenzocoronenium graphene nanoribbons through on-surface synthesis and elucidated their electronic structure and charge state experimentally and theoretically. The present versatile approach opens up new possibilities for the utilization of heteroatom-embedded hexabenzocoronene derivatives in various potential applications.

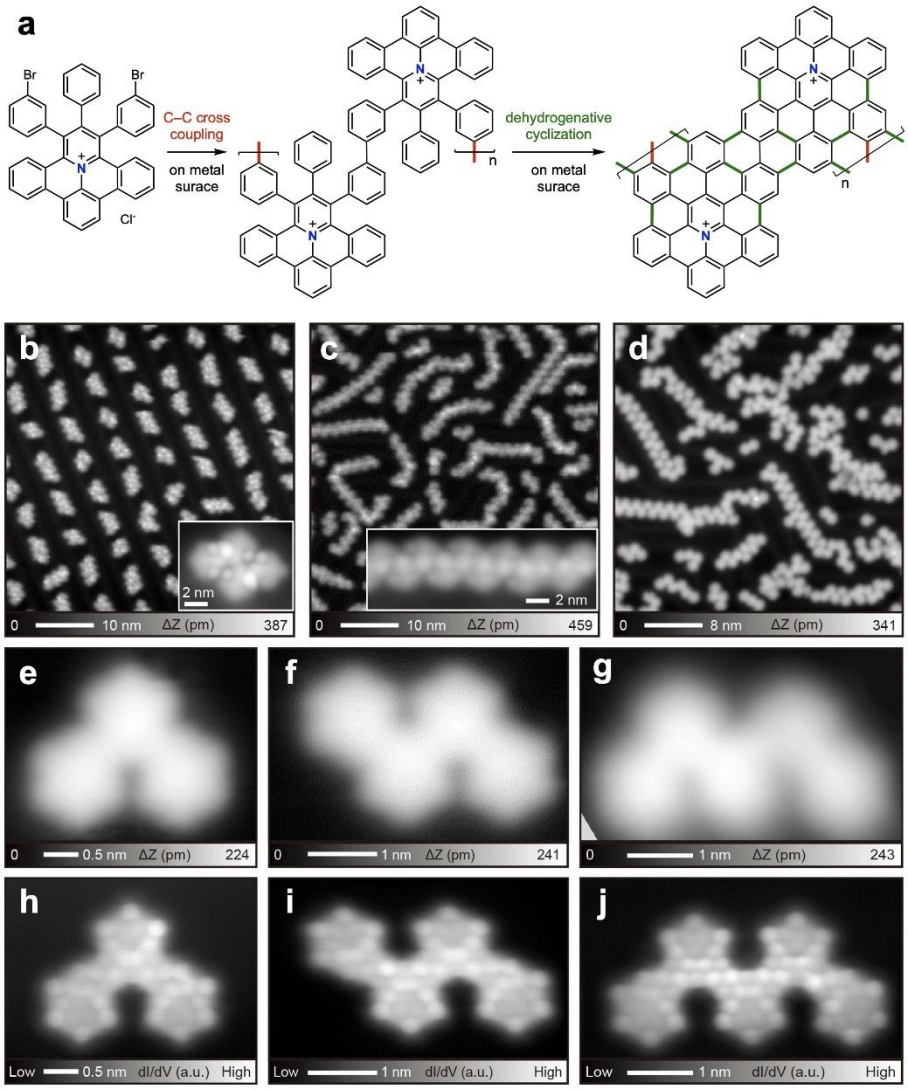

Fig. 7. On-surface synthesis of aza-HBC-based corrugated graphene nanoribbons. a, On-surface oligomerization of azahexabenzocoronenium precursor **4d** via Ullmann-type coupling and cyclodehydrogenation. **b**, Overview STM topography of as-deposited **4d** on Au(111). Inset, high-resolution STM image of the self-assembled clusters. **c**, Overview STM topography after annealing at 150 °C. Inset, high-resolution STM image of the polymer. **d**, Overview STM topography after annealing at 400 °C. **e–g**, High-resolution STM images of GNRs. **h–j**, Bond-resolved STM (BR-STM) images of GNRs. Measurement parameters: V = 200 mV and I = 10 pA in (b–g), and V = 0 mV in (h–j).

Methods

1,3-Dipolar cycloaddition of azomethine ylides 1 and cyclopropenes 2: To a preheated solution of cyclopropene **2** (0.10 mmol) and iminium salt **1** (0.15 mmol) in dimethyl sulfoxide (3.0 mL) at 120 °C was added *N*,*N*-diisopropyl(ethyl)amine (0.45 mmol). The mixture was stirred for 14 h at 120 °C, cooled to room temperature and poured into toluene (30 mL). The organic phase was washed with brine (10 mL×3), dried over sodium sulfate and concentrated under reduced pressure. The crude mixture was purified by silica gel chromatography to obtain cycloadduct **3** as a mixture of diastereomers.

Oxidative aromatization of 3 to synthesize π-extended pyridinium 4: To a solution of compound **3** (0.050 mmol, a mixture of stereoisomers) in chloroform (3.0 mL) was added chloranil (0.15 mmol) at room temperature. The mixture was stirred for 3 h at 40 °C and cooled to room temperature. After being concentrated under reduced pressure, the crude mixture was purified by silica-gel chromatography (methanol/dichloromethane) to obtain π-extended pyridinium **4**.

Mechanochemical cyclization of 4 to synthesize azahexabenzocoronenium 5: To a 15-mL stainless steel jar was placed **4** (10 mg, 13–14 μmol), sodium (10 mg, 0.4 mmol) and a stainless-steel ball. The jar was closed and milled at 30 Hz for 30 min. The reaction mixture was collected with chloroform and the organic layers were concentrated under reduced pressure. The crude mixture was purified by silica-gel column chromatography (methanol/dichloromethane) to obtain azahexabenzocoronenium **5**.

Data availability

The crystallographic data for compounds **3a**, **4a**, and **5h'** have been deposited with the Cambridge Crystallographic Data Centre under accession numbers **2293773**, **2293774**, and **2293775**, respectively. The data supporting the findings of the current study are available within the paper and its Supplementary Information.

Acknowledgements

This work was supported by Nanyang Technological University (NTU), the Ministry of Education, Singapore, under its Academic Research Fund Tier 1 (RG2/23) for S.I. and the Japan Society for the Promotion of Science (JSPS) KAKENHI Grant Number 22H00285 for S.K. Computing resources from the NTU High Performance Computing Team are gratefully acknowledged. We thank Dr. Yongxin Li (NTU) for his support with the X-ray diffraction analysis and Dr. Orlando J. Silveira (Aalto University) for valuable discussion on the theoretical calculations.

Author contributions

S.I. directed and conceived the project and performed the theoretical studies with DFT calculations. X.Z., C.C.H.T, F.H., and Y.H. performed all the experimental work and data collection in organic synthesis. D.L. and S.K. performed the scanning tunneling microscopy experiments and analyzed the results. A.S.F performed theoretical calculations of the corrugated GNRs deposited on the metal surface. All the authors discussed the results and contributed to the preparation of the manuscript.

Competing interests

The authors declare no competing interests.

References

[1] Clar, E. & Ironside, C. T. Hexabenzocoronene. *Proc. Chem. Soc.* 150 (1958).

[2] Clar, E., Ironside, C. T., & Zander, M. The electronic interaction between benzenoid rings in condensed aromatic hydrocarbons. 1:12-2:3-4:5-6:7-8:9-10:11-hexabenzocoronene, 1:2-3:4-5:6-10:11-tetrabenzoanthanthrene, and 4:5-6:7-11:12-13:14-tetrabenzoperopyrene. *J. Chem. Soc.* 142–147 (1959).

[3] Wu, J., Pisula, W. & Müllen, K. Graphenes as potential material for electronics, *Chem. Rev.* **107**, 718–747 (2007).

[4] Seyler, H., Purushothaman, B., Jones, D. J., Holmes, A. B. & Wong, W. W. H. Hexa-*peri*-hexabenzocoronene in organic electronics, *Pure Appl. Chem.* **84**, 1047–1067 (2012).

[5] Kumar, S. & Tao, Y.-T. Coronenes, benzocoronenes and beyond: modern aspects of their syntheses, properties, and applications. *Chem. Asian J.* **16**, 621–647 (2021).

[6] Hill, J. P., Jin, W., Kosaka, A., Fukushima, T., Ichihara, H., Shimomura, T., Ito, K., Hashizume, T., Ishii, N. & Aida, T. Self-assembled hexa-*peri*-hexabenzocoronene graphitic nanotube, *Science* **304**, 1481–1483 (2004).

[7] For a review, see: Ishiwari, F., Shoji, Y. & Fukushima, T. Supramolecular scaffolds enabling the controlled assembly of functional molecular units. *Chem. Sci.* **9**, 2028–2041 (2018).

[8] Lin, F.-J., Chen, H.-H. & Tao, Y.-T. Molecularly aligned hexa-*peri*-hexabenzocoronene films by brush-coating and their application in thin-film transistors. *ACS Appl. Mater. Interfaces* **11**, 10801−10809 (2019).

[9] Lin, F.-J., Yang, C.-W., Chen, H.-H. & Tao, Y.-T. Alignment and photopolymerization of hexa-peri-hexabenzocoronene derivatives carrying diacetylenic side chains for charge-transporting application. *J. Am. Chem. Soc.* **142**, 11763–11771 (2020).

[10] Yin, M., Shen, J., Pisula, W., Liang, M., Zhi, L. & Müllen, K. Functionalization of self-assembled hexa-*peri*-hexabenzocoronene fibers with peptides for bioprobing. *J. Am. Chem. Soc.* **131**, 14618–14619 (2009).

[11] Zilberman, Y., Tisch, U., Shuster, G., Pisula, W., Feng, X., Müllen, K. & Haick, H. Carbon nanotube/hexa-*peri*-hexabenzocoronene bilayers for discrimination between nonpolar volatile organic compounds of cancer and humid atmospheres. *Adv. Mater.* **22**, 4317–4320 (2010).

[12] Stępień, M., Gońka, E., Żyła, M. & Sprutta, N. Heterocyclic nanographenes and other polycyclic heteroaromatic compounds: synthetic routes, properties, and applications. *Chem. Rev.* **117**, 3479–3716 (2017).

[13] Wang, X.-Y., Yao, X., Narita, A. & Müllen, K. Heteroatom-doped nanographenes with structural precision. *Acc. Chem. Res.* **52**, 2491–2505 (2019).

[14] Borissov, A., Maurya, Y. K., Moshniaha, L., Wong, W.-S., Żyła-Karwowska, M. & Stępień, M. Recent advances in heterocyclic nanographenes and other polycyclic heteroaromatic compounds. *Chem. Rev.* **122**, 565–788 (2022).

[15] Draper, S. M., Gregg, D. J. & Madathil, R. Heterosuperbenzenes: a new family of nitrogen-functionalized, graphitic molecules, *J. Am. Chem. Soc.* **124**, 3486–3487 (2002).

[16] Draper, S. M., Gregg, D. J., Schofield, E. R., Browne, W. R., Duati, M., Vos, J. G. & Passaniti, P. Complexed nitrogen heterosuperbenzene: the coordinating properties of a remarkable ligand. *J. Am. Chem. Soc.* **126**, 8694–8701 (2004).

[17] Wijesinghe, L. P., Perera, S. D., Larkin, E., Ó Máille, G. M., Conway-Kenny, R., Lankage, B. S., Wang, L. & Draper, S. M. [2 + 2 + 2] Cyclotrimerisation as a convenient route to 6N-doped nanographenes: a synthetic introduction to hexaazasuperbenzenes. *RSC Adv.* **7**, 24163–24167 (2017).

[18] Graczyk, A., Murphy, F. A., Nolan, D., Fernández-Moreira, V., Lundin, N. J., Fitchett, C. M. & Draper, S. M. Terpyridine-fused polyaromatic hydrocarbons generated via cyclodehydrogenation and used as ligands in Ru(II) complexes. *Dalton Trans.* **41**, 7746–7754 (2012).

[19] Reger, D., Schöll, K., Hampel, F., Maid, H. & Jux, N. Pyridinic nanographenes by novel precursor design. *Chem. Eur. J.* **27**, 1984–1989 (2021).

[20] Krieg, M., Reicherter, F., Haiss, P., Ströbele, M., Eichele, K., Treanor, M.-J., Schaub, R. & Bettinger, H. F. Construction of an internally B_3N_3-doped nanographene molecule. *Angew. Chem. Int. Ed.* **54**, 8284–8286 (2015).

[21] Wang, X.-Y., Richter, M., He, Y., Björk, J., Riss, A., Rajesh, R., Garnica, M., Hennersdorf, F., Weigand, J. J., Narita, A., Berger, R., Feng, X., Auwärter, W., Barth, J. V., Palma, C.-A. & Müllen, K. Exploration of pyrazine-embedded antiaromatic polycyclic hydrocarbons generated by solution and on-surface azomethine ylide homocoupling. *Nat. Commun.* 8:1948 (2017).

[22] Biswas, K., Urgel, J. I., Xu, K., Ma, J., Sánchez-Grande, A., Mutombo, P., Gallardo, A., Lauwaet, K., Mallada, B., de la Torre, B., Matěj, A., Gallego, J. M., Miranda, R., Jelínek, P., Feng, X. & Écija , D. On-surface synthesis of a dicationic diazahexabenzocoronene derivative on the Au(111) surface. *Angew. Chem. Int. Ed.* **60**, 25551−25556 (2021).

[23] Dosso, J., Tasseroul, J., Fasano, F., Marinelli, D., Biot, N., Fermi, A. & Bonifazi, D. Synthesis and optoelectronic properties of hexa-*peri*-hexabenzoborazinocoronene. *Angew. Chem. Int. Ed.* **56**, 4483–4487 (2017).

[24] Dosso, J., Battisti, T., Ward, B. D., Demitri, N., Hughes, C. E., Williams, P. A., Harris, K. D. M. & Bonifazi, D. Boron–nitrogen-doped nanographenes: a synthetic tale from borazine precursors. *Chem. Eur. J.* **26**, 6608–6621 (2019).

[25] Berger, R., Giannakopoulos, A., Ravat, P., Wagner, M., Beljonne, D., Feng, X. & Müllen, K. Synthesis of nitrogen-doped zigzag-edge peripheries: dibenzo-9*a*-azaphenalene as repeating unit. *Angew. Chem. Int. Ed.* **53**, 10520–10524 (2014).

[26] Ito, S., Tokimaru, Y. & Nozaki, K. Isoquinolino[4,3,2-*de*]phenanthridine: synthesis and its use in 1,3-dipolar cycloadditions to form nitrogen-containing polyaromatic hydrocarbons. *Chem. Commun.* **51**, 221–224 (2015).

[27] Berger, R., Wagner, M., Feng, X. & Müllen, K. Polycyclic aromatic azomethine ylides: a unique entry to extended polycyclic heteroaromatics. *Chem. Sci.* **6**, 436–441 (2015).

[28] Tokimaru, Y., Ito, S. &. Nozaki, K. Synthesis of pyrrole-fused corannulenes: 1,3-dipolar cycloaddition of azomethine ylides to corannulene. *Angew. Chem. Int. Ed.* **56**, 15560–15564 (2017).

[29] Dumele, O., Đorđević, L., Sai, H., Cotey, T. J., Sangji, M. H., Sato, K., Dannenhoffer, A. J. & Stupp, S. I. Photocatalytic aqueous CO_2 reduction to CO and CH_4 sensitized by ullazine supramolecular polymers. *J. Am. Chem. Soc.* **144**, 3127–3136 (2022).

[30] Zhang, X. Mackinnon, M. R., Bodwell, G. J. & S. Ito, S. Synthesis of a π-extended azacorannulenophane enabled by strain-Induced 1,3-dipolar cycloaddition. *Angew. Chem. Int. Ed.* **61**, e202116585 (2022).

[31] Li, S., Sun, Y., Li, X., Smaga, O., Koniarz, S., Stępień, M. & Chmielewski, P. J. 1,3-Dipolar cycloaddition of polycyclic azomethine ylide to norcorroles: towards dibenzoullazine-fused derivatives. *Chem. Commun.* **58**, 6510–6513 (2022).

[32] Hager, J., Kang, S., Chmielewski, P. J., Lis, T., Kim, D. & Stępień, M. Acenaphthylene-fused ullazines: fluorescent π-extended monopyrroles with tunable electronic gaps. *Org. Chem. Front.* **9**, 3179–3185 (2022).

[33] Ikeda, H., Hoshi, Y. & Miyashi, T. 1,3-Bis(4-methoxyphenyl)cyclohexane-1,3-diyl cation radical: divergent reactivity depending upon electron-transfer conditions. *Tetrahedron Lett.* **42**, 8485–8488 (2001).

[34] Gaucher, X., Jida, M. & Ollivier, J. Concise total asymmetric synthesis of (*S*)-2-phenylpiperidin-3-one. *Synlett* **20**, 3320–3322 (2009).

[35] Xu, W.-B., Li, C. & Wang, J. Rh^{I}-catalyzed carbonylative [3+1] construction of cyclobutenones via C−C σ-bond activation of cyclopropenes. *Chem. Eur. J.* **24**, 15786–15790 (2018).

[36] Grzybowski, M., Skonieczny, K., Butenschön, H. & Gryko, D. T. Comparison of oxidative aromatic coupling and the Scholl reaction. *Angew. Chem. Int. Ed.* **52**, 9900–9930 (2013).

[37] Grzybowski, M., Sadowski, B., Butenschön, H. & Gryko, D. T. Synthetic applications of oxidative aromatic coupling—from biphenols to nanographenes. *Angew. Chem. Int. Ed.* **59**, 2998–3027 (2020).

[38] Jassas, R. S., Mughal, E. U., Sadiq, A., Alsantali, R. I., Al-Rooqi, M. M., Naeem, N., Moussa, Z. & Ahmed, S. A. Scholl reaction as a powerful tool for the synthesis of nanographenes: a systematic review. *RSC Adv.* **11**, 32158–32202 (2021).

[39] Schlichting, P., Rohr, U. & Müllen, K. Easy synthesis of liquid crystalline perylene derivatives. *J. Mater. Chem.* **8**, 2651–2655 (1998).

[40] Gryko, D. T., Piechowska, J. & Gałęzowski, M. Strongly emitting fluorophores based on 1-azaperylene scaffold. *J. Org. Chem.* **75**, 1297–1300 (2010).

[41] Rickhaus, M., Belanger, A. P., Wegner, H. A. & Scott, L. T. An oxidation induced by potassium metal. Studies on the anionic cyclodehydrogenation of 1,1'-binaphthyl to perylene. *J. Org. Chem.* **75**, 7358–7364 (2010).

[42] Kawahara, K. P., Matsuoka, W., Ito, H. & Itami, K. Synthesis of nitrogen-containing polyaromatics by aza-annulative π-extension of unfunctionalized aromatics. *Angew. Chem. Int. Ed.* **59**, 6383–6388 (2020).

[43] Wang, C.-S., Sun, Q., García, F., Wang, C. & Yoshikai, N. Robust cobalt catalyst for nitrile/alkyne [2+2+2] cycloaddition: synthesis of polyarylpyridines and their mechanochemical cyclodehydrogenation to nitrogen-containing polyaromatics. *Angew. Chem. Int. Ed.* **60**, 9627–9634 (2021).

[44] Herwig, P. T., Enkelmann, V., Schmelz, O. & Müllen, K. Synthesis and structural characterization of hexa-*tert*-butyl-hexa-*peri*-hexabenzocoronene, its radical cation salt and its tricarbonylchromium complex. *Chem. Eur. J.* **6**, 1834–1839 (2020).

[45] Nagase, M., Kato, K., Yagi, Y., Segawa, Y. & Itami, K. Six-fold C–H borylation of hexa-*peri*-hexabenzocoronene. *Beilstein J. Org. Chem.* **16**, 391–397 (2020).

[46] Hu, Y., Wang, D., Baumgarten, M., Schollmeyer, D., Müllen, K. & Narita, A. Spiro-fused bis-hexa-*peri*-hexabenzocoronene. *Chem. Commun.* **54**, 13575–13578 (2018).

[47] Kastler, M., Schmidt, J., Pisula, W., Sebastiani, D. & Müllen, K. From armchair to zigzag peripheries in nanographenes. *J. Am. Chem. Soc.* **128**, 9526–9534 (2006).

[48] Ito, S., Tokimaru, Y., & Nozaki, K. Benzene-fused azacorannulene bearing an internal nitrogen atom. *Angew. Chem. Int. Ed.* **54**, 7256–7260 (2015).

[49] Bronner, C., Stremlau, S., Gille, M., Braußе, F., Haase, A., Hecht, S. & Tegeder, P. Aligning the band gap of graphene nanoribbons by monomer doping. *Angew. Chem. Int. Ed.* **52**, 4422–4425 (2013).

[50] Vo, T. H., Shekhirev, M., Kunkel, D. A., Orange, F., Guinel, M. J.-F., Enders, A. & Sinitskii, A. Bottom-up solution synthesis of narrow nitrogen-doped graphene nanoribbons. *Chem. Commun.* **50**, 4172–4174 (2014).

[51] Zhang, Y., Zhang, Y., Li, G., Lu, J., Lin, X., Du, S., Berger, R., Feng, X., Müllen, K. & Gao, H.-J. Direct visualization of atomically precise nitrogen-doped graphene nanoribbons. *Appl. Phys. Lett.* **105**, 023101 (2014).

[52] Cai, J. Pignedoli, C. A., Talirz, L., Ruffieux, P., Söde, H., Liang, L., Meunier, V., Berger, R., Li, R., Feng, X., Müllen, K. & Fasel, R. Graphene nanoribbon heterojunctions. *Nat. Nanotechnol.* **9**, 896–900 (2014).

[53] Vo, T. H., Perera, U. G. E., Shekhirev, M., Pour, M. M., Kunkel, D. A., Lu, H., Gruverman, A., Sutter, E., Cotlet, M., Nykypanchuk, D., Zahl, P., Enders, A., Sinitskii, A., & Sutter, P. Nitrogen-doping induced self-assembly of graphene nanoribbon-based two-dimensional and three-dimensional metamaterials. *Nano. Lett.* **15**, 5770–5777 (2015).

[54] Marangoni, T., Haberer, D., Rizzo, D. J., Cloke, R. R. & Fischer, F. R. Heterostructures through divergent edge reconstruction in nitrogen-doped segmented graphene nanoribbons. *Chem. Eur. J.* **22**, 13037–13040 (2016).

[55] Durr, R. A., Haberer, D., Lee, Y.-L., Blackwell, R., Kalayjian, A. M., Marangoni, T., Ihm, J., Louie, S. G. & Fischer, F. R. Orbitally matched edge-doping in graphene nanoribbons. *J. Am. Chem. Soc.* **140**, 807–813 (2018).

[56] Wen, E. C. H., Jacobse, P. H., Jiang, J., Wang, Z., McCurdy, R. D., Louie, S. G., Crommie, M. F. & Fischer, F. R. Magnetic interactions in substitutional core-doped graphene nanoribbons. *J. Am. Chem. Soc.* **144**, 13696–13703 (2022).

[57] Wang, T., Berdonces-Layunta, A., Friedrich, N., Vilas-Varela, M., Calupitan, J. P., Pascual, J. I., Peña, D., Casanova, D., Corso, M. & de Oteyza, D. G. Aza-triangulene: on-surface synthesis and electronic and magnetic properties. *J. Am. Chem. Soc.* **144**, 4522–4529 (2022).

[58] Lawrence, J., He, Y., Wei, H., Su, J., Song, S., Rodrigues, A. W., Miravet, D., Hawrylak, P., Zhao, J., Wu, J. & Lu, J. Topological design and synthesis of high-spin aza-triangulenes without Jahn–Teller distortions. *ACS Nano* **17**, 20237–20245 (2023).